Vol. 732: 53–71, 2024
https://doi.org/10.3354/meps14545

MARINE ECOLOGY PROGRESS SERIES
Mar Ecol Prog Ser

Published March 20

Edge effects of a fragmented seagrass habitat on flow, bivalve recruitment, and sediment dynamics

Elise Turrietta, Matthew A. Reidenbach*

Department of Environmental Sciences, University of Virginia, Charlottesville, Virginia 22904, USA

ABSTRACT: In both continuous and fragmented seagrass ecosystems, the vegetation edge can be a location of abrupt hydrodynamic change, with impacts to both ecological and physical processes. We address how flow and wave activity change across seagrass meadow edges and the effects of vegetation on sediment dynamics and bivalve recruitment. Two *Zostera marina* seagrass meadow sites were monitored: a high-density site with >500 shoots m^{-2} and a low-density site with <250 shoots m^{-2}. Mean flow velocities were significantly reduced in seagrass vegetation adjacent to edges, with reductions compared to unvegetated areas ranging from 30–75%. Recruitment of juvenile bivalves was significantly elevated within vegetation. No significant differences in wave activity or sediment suspension and/or deposition were found spatially across a 10 m distance from a seagrass edge, but significant temporal variability was observed, caused by periodic storms. Wave height was a major predictor for sediment movement along seagrass edges, with an observed 10-fold increase in sediment collection within benthic traps following severe storms. These results were found across various heterogeneous edge configurations and reveal abrupt hydrodynamic responses of both mean flow and turbulence to occur at short spatial scales (1–10 m), with changes to wave and sediment deposition and/or suspension conditions only occurring over larger spatial distances (~100 m). Changes to the hydrodynamic regime were therefore found to be driven by meteorological conditions (e.g. winds, storms) on daily timescales and by changes in seagrass shoot density, altering both bivalve recruitment and sediment dynamics on longer temporal and/or spatial timescales.

KEY WORDS: Seagrass · Hydrodynamics · Bivalve larvae · Sediment resuspension · Fragmentation · Recruitment

1. INTRODUCTION

Seagrass meadows provide an extensive range of ecosystem services, including coastal protection, faunal habitats, carbon sequestration, and enhanced water quality (Aoki et al. 2020, Oreska et al. 2020). However, as human development and use of coastal landscapes increase along with a warming climate (Allen et al. 2021), seagrass ecosystems have been degraded globally (Dunic et al. 2021). This degradation has spurred restoration efforts and has simultaneously generated questions regarding how alterations of these vegetated environments lead to ecological and physical consequences and state changes (McGlathery et al. 2013). Seagrasses also have an extensive influence on hydrodynamic patterns by inducing drag on the surrounding flow. This leads to velocity gradients and the formation of boundary layers at several spatial scales, from turbulence generation around individual blades to reduced flow across an entire meadow (Koch et al. 2006, Nepf 2012, Reidenbach & Thomas 2018).

1.1. Flow conditions in seagrass

Within the canopy, Hansen & Reidenbach (2012) found seagrass presence to reduce near-bottom mean velocities by up to 90% compared to unvegetated regions. The induced drag also alters velocity profiles, as a shear layer forms at the interface of the canopy and overlying water (Gambi et al. 1990), creating regions

*Corresponding author: mar5jj@virginia.edu

of increased velocity above the top of the canopy and reduced flow below it (Ghisalberti & Nepf 2002). At high seagrass densities, 'skimming flow' can occur, whereby increased velocity above the canopy arises as the amount of bulk water flow through the canopy is substantially reduced (Koch & Gust 1999, Hansen & Reidenbach 2017). Seagrass density and patch morphology also influence turbulence regimes, with high blade densities (>500 shoots m^{-2}) resulting in a stronger turbulent shear layer above the canopy and reduced mixing below it (Nepf & Vivoni 2000, Hansen & Reidenbach 2012). However, at low densities (<200 shoots m^{-2}), flow can penetrate within the canopy and increase turbulence caused by stem–wake interactions (Fonseca & Koehl 2006, Hansen & Reidenbach 2013).

It has been well established that seagrass presence also results in wave attenuation (Twomey et al. 2020). However, the degree of attenuation depends on whether the prevailing flow conditions are driven by winds or tidally driven currents (Zhu et al. 2021), and the characteristics of the waves influence the extent of seagrass response (Bradley & Houser 2009). Results from both modeling and experimental studies have shown that higher seagrass density and biomass leads to greater attenuation in wave height but depends upon the spatial extent of the meadow (Chen et al. 2007, Bradley & Houser 2009), with Reidenbach & Thomas (2018) showing attenuation of wave heights across hundreds of meters of meadow. At the smaller patch scale, El Allaoui et al. (2016) found that more fragmented canopies resulted in less attenuation of waves and increased mean flow velocities and that fragmented seagrass environments are less efficient at providing a sheltering habitat against high flow conditions. Theoretical, laboratory, and field studies have also shown that substantial reductions of in-canopy velocities are expected for mean flows or for low-frequency waves when the orbital excursions are larger than the canopy drag length scale, which is a function of seagrass blade geometry and spacing (Lowe et al. 2005, 2007, Luhar et al. 2010). However, little is known about how changes to flow conditions along a fragmented seagrass landscape occur that might impact sediment and larval settlement dynamics on both short-term (wave-driven storm conditions) and longer-term (spring–neap tidal cycles) hydrodynamic forcings.

1.2. Hydrodynamic impacts on sediment suspension and deposition

Generally, oscillatory motions caused by waves penetrate deeper into the seagrass canopy than tidally driven flow and can interact with the seafloor to create a velocity gradient at the sediment–water interface (Koch & Gust 1999, Hansen & Reidenbach 2012). The presence of waves, when combined with current flow, results in a separate, combined wave–current boundary layer (Grant & Madsen 1979), which enhances bottom shear stresses that can exceed the critical stress threshold necessary for sediment resuspension (Reidenbach & Timmerman 2019). The strength of the bed shear formed at the sediment–water interface often determines local suspended sediment concentrations (SSCs) (Lawson et al. 2007), while tidal currents largely control the net sediment transport through the system at large (Jing & Ridd 1996). The presence of seagrass alters the magnitude of these flow–sediment interactions (Donatelli et al. 2018, Zhu et al. 2022). Hansen & Reidenbach (2012) found that in a combined wave–current flow, bed shear stress in bare areas often exceeded the critical stress threshold to initiate sediment movement, whereas at vegetated sites, the bed shear stress was lower than this critical value 80% of the time. The reduction in sediment resuspension within seagrass ecosystems can be attributed to the reduction in canopy flow velocity as well as sediment stabilization by the seagrass roots (Gacia & Duarte 2001, Nardin et al. 2018).

Because of this limited resuspension, seagrass meadows are often considered depositional environments for sediment, which may create a positive feedback loop whereby more light availability encourages more seagrass growth, further reducing SSCs (Adams et al. 2016). Recent work by Zhu et al. (2021) modeled the effects of flow–wave–vegetation interaction at a meadow scale and concluded that vegetation density mediated the response of SSCs and sediment transport. Seasonally, higher density vegetation in the summer (>200 shoots m^{-2}) significantly attenuated flow, waves, and SSCs, but lower density vegetation (<160 shoots m^{-2}) in the winter resulted in much smaller SSC reductions. Under similar conditions, meadow edges were the most sensitive to changes in erosional or depositional conditions and controlled the amount of suspended sediment advected throughout the system at large (Zhu et al. 2022).

1.3. Bivalve settlement, recruitment, and abundance

In addition to their pronounced effect on flow regimes, seagrass presence has been linked to increased species richness, diversity, density, and

abundance of associated macrofauna (Orth et al. 1984, Bologna & Heck 2002). Studies have shown significant positive correlations between bivalve abundance and seagrass density and biomass (Peterson et al. 1984, Glaspie & Seitz 2017). Based on these results, there has been effort to show that the positive relationship between seagrasses and bivalves depends on the surrounding hydrodynamic conditions that alter dispersal and settlement patterns (Eckman 1983, Irlandi 1997). In addition to actively swimming larvae (Koehl & Reidenbach 2007), many benthic invertebrates have planktonic larvae that passively settle in turbulent flow environments (Butman 1989, Koehl & Hadfield 2010). Studies have shown that seagrasses may trap these passive larvae just as they trap sediment and that bivalve settlement patterns may be associated with seagrass presence and canopy structure, which alters flow (Eckman 1983, Bologna & Heck 2002).

Bay scallops *Agropecten irradians*, for example, have an extremely close association with seagrass beds by nature of their settlement method (Carroll et al. 2012). Eckman (1987) studied the influence of hydrodynamic forces on the recruitment, growth, and survival of bay scallops, concluding that the altered hydrodynamics of eelgrass *Zostera marina* beds significantly affected larval recruitment to a higher degree than predation or inter-blade abrasion. Hydrodynamics also influence the settlement and recruitment of hard clams *Mercenaria mercenaria*, with increased clam population density and individual growth rates linked to seagrass presence (Peterson et al. 1984). The seagrass-induced impact of local hydrodynamics on passively settling larvae explained differences in clam densities between bare and vegetated sites, even when accounting for altered post-settlement survival.

Based on these and other studies, landscape ecology has become an increasingly important approach for examining the effects of seagrass on bivalve distribution. Differences in the spatial patterning of a seagrass meadow (in terms of percent cover) can influence the distribution and abundance of faunal inhabitants and alter trophic interactions (McCloskey & Unsworth 2015). The influence of fragmented seagrass habitats on its associated fauna is extremely variable but not always negative, as traditionally thought (Carroll et al. 2012), and previous work suggests that fauna along seagrass edges may experience tradeoffs to balance counteracting influences of both enhanced settlement and predation (Bologna & Heck 2002). This may be due to a 'settlement shadow' in which, due to the decrease in current speed through a seagrass canopy, particle settlement should be greatest at a canopy edge and decrease into the meadow. This trend was experimentally observed in bivalve larvae by Bologna & Heck (2000), who found significantly greater larval densities at seagrass patch edges.

1.4. Seagrass fragmentation and landscape dynamics

Anthropogenic influence from coastal development and a simultaneously warming climate have accelerated the rate of seagrass ecosystem loss (Dunic et al. 2021). This degradation drives not only ecosystem loss but also fragmentation, leading to a more discontinuous habitat (Yarnall et al. 2022). While the natural edges of seagrass meadows have previously been viewed as a 'presence vs. absence' dichotomy of vegetation, the increased prevalence of edges across fragmented seagrass ecosystems can impact hydrodynamics and sediment movement on both small and large spatial scales (Colomer et al. 2017, Zhu et al. 2022). However, research addressing varied seagrass landscape structure at a range of scales has yielded inconsistent results regarding the relationships between flow regime, sediment transport, and faunal distribution. There remain unanswered questions as to how these dynamics persist over a variety of edge settings, including that of a homogeneous meadow or those that characterize fragmented or heterogeneous landscapes. This research, therefore, addresses the following questions: (1) How do hydrodynamic conditions and wave activity change across edges of seagrass vegetation at the meadow scale and in fragmented landscapes? (2) How do these altered flow conditions influence sediment deposition and transport? (3) Does bivalve settlement and recruitment vary in response to these flow changes?

2. MATERIALS AND METHODS

2.1. Study site

Field studies were conducted in South Bay, a coastal lagoon set behind barrier islands bordering the east side of the Delmarva Peninsula, Virginia, USA (Fig. 1). This shallow bay is part of the National Science Foundation's Virginia Coast Reserve Long Term Ecological Research (VCR LTER) site that consists of several coastal bays and their interconnected salt marshes, ocean inlets, and barrier islands. South

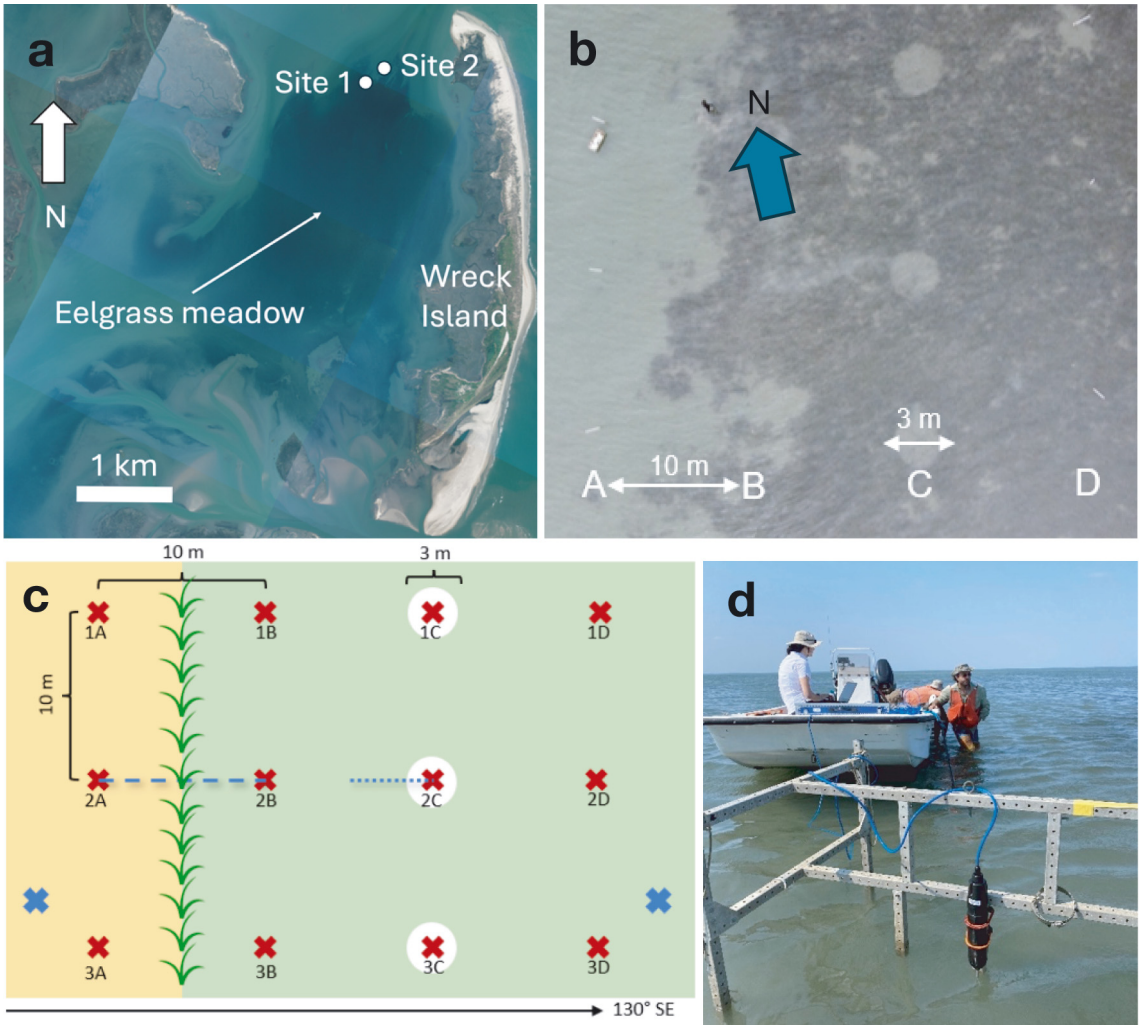

Fig. 1. (a) Aerial image of study locations Site 1 (37.2786° N, 75.8113° W) and Site 2 (37.2791° N, 75.8108° W) along the northern edge of South Bay eelgrass meadow. The extent of the eelgrass meadow can be seen as dark regions within the bay to the west of Wreck barrier island. (b) Aerial photo of Site 1 showing the 4 sampling locations (A–D) along 3 parallel transects, including manmade bare patches at the C locations. (c) Schematic of Site 1 sampling array with 3 parallel transects (1–3) heading 130° SE from naturally unvegetated seafloor (yellow) past the meadow's edge into vegetation (green), each with 4 replicative, designated locations (A–D) for bivalve and sediment sampling (red '×'s). Site 1C locations occur in manmade bare patches of 3 m diameter (white). Hydrodynamic sampling occurred along smaller transects and at site perimeters (blue dashes, blue '×'s). (d) Image of Vectrino on frame used to compute transect velocities

Bay has an approximate area of 31.5 km^2 with an average depth of roughly 1.0 m and a tidal range between 0.5 and 1.5 m (Reidenbach & Thomas 2018). Due to the shallow depth, low freshwater inputs, and narrow ocean channels into South Bay, turbidity is primarily caused by sediment resuspension induced by wind-driven waves and transport driven by tidal currents (Lawson et al. 2007, Fagherazzi & Wiberg 2009). High concentrations of resuspended sediment may limit light penetration through the water column, with resulting decreases in primary productivity (McGlathery et al. 2001).

The shallow coastal lagoons of the Delmarva Peninsula were once dominated by *Zostera marina* eelgrass. A combination of disease and extreme weather in the early 1930s led to local elimination of *Z. marina*. However, when natural occurrences of *Z. marina* were discovered in the 1990s, systematic restoration efforts began in several coastal bays including South Bay, and this work has been largely successful with continued meadow reseeding and growth (Oreska et al. 2021). Seeds were initially broadcasted in South Bay in 0.4 ha plots, beginning in 2001, and over subsequent years have coalesced into a continuous meadow of

7 km^2 as of 2015. However, a large seagrass die-off occurred in 2015, linked to a marine heat wave (Aoki et al. 2021), which has altered the spatial distribution of the meadow and impacted seagrass restoration success. Seagrass recovery has subsequently occurred in South Bay, and meadow expansion continues to change the fluid dynamics within this system (Reidenbach & Thomas 2018). Seagrasses within the system typically reach a maximum shoot density of >500 m^{-2} in early summer and a minimum of 50–100 m^{-2} during winter senescence (Berger et al. 2020).

In 2021, a study area (Site 1) was selected on the northern edge of the South Bay eelgrass meadow (Fig. 1b). Three replicate transects were delineated along a 130° trajectory roughly perpendicular to the dominant north–south flow direction of South Bay. Each transect had 4 sampling locations (locations A–D) for sediment, bivalve, and hydrodynamic conditions within (A) in naturally unvegetated seafloor, (B) 5 m from the vegetation edge within meadow, and (D) 25 m from the vegetation edge within meadow. All (C) sampling locations were located within a patch of bare seafloor where seagrass was manually removed from a circular area 3 m in diameter and located 15 m from the seagrass edge (Fig. 1b). This location was used to simulate fragmentation and address how bare patches and edges of discontinuous seagrass cover contribute to alterations of local flow conditions and sediment dynamics. Site 1 was characterized as having a dense seagrass cover that ranged from 480 to 680 shoots m^{-2} during sampling, with an average of 555 ± 75 shoots m^{-2}.

In 2022, a second study area (Site 2) was chosen to conduct additional sampling at a region within the canopy considered to have low seagrass density, ranging between 150 and 245 shoots m^{-2} during periods of sampling, with an average (±1 SD) of 200 ± 50 shoots m^{-2}. On average, blade length was 48 ± 8 (SD) cm and blade width was 0.35 cm, with a submerged canopy height of approximately 30 cm. The canopy was consistently subtidal, with average water depths across sites and sampling periods ranging between 1.04 and 1.95 m and low tide depths of approximately 0.5 m. Site 2 was located approximately 100 m to the northeast of Site 1 and similarly positioned along the northern edge of the South Bay seagrass meadow (Fig. 1). One transect was delineated at Site 2 with 3 designated sampling locations (locations A, B, and E). Location A was in naturally bare seafloor 5 m from the edge, and location B was within the seagrass meadow 5 m from the edge, similar to Site 1. Location E was located 100 m into the seagrass canopy. This transect ran roughly perpendicular to the meadow's edge in this location (along a 150° trajectory) and along South Bay's dominant flow direction. No bare patches were created at Site 2, but repeated sampling was performed at Site 1 in 2022 at all 4 locations.

2.2. Hydrodynamic instrumentation

To assess differences in wave characteristics across the meadow's edge, wave gauges (Richard Branker Research RBRduo^3) were concurrently deployed during multiple 2–3 wk deployments, for nearly continuous recordings from May through August 2021 at Site 1. These instruments were fastened to weighted metal frames 10 m apart, one positioned in the naturally bare seafloor at location A and one in full vegetation at location B. To maximize data quality with battery and instrument memory limitations, instruments were programmed to record wave height measurements every 10 min at 4 Hz for bursts of 1024 samples (i.e. 256 s of data), which were averaged to produce a mean value every 10 min. Measurements include water depth, tidal slope, and significant wave height (H_s). These instruments were again deployed in summer 2022 at Site 2 in locations A and B.

Two high-resolution Nortek Aquadopp acoustic Doppler current profilers (ADCPs) were used to quantify flow conditions in 2021 at Site 1 in bare and vegetated sampling locations (locations A and D), and in 2022 at Site 2 (locations A and E). Instruments were positioned on the seafloor at z = 5 cm in an upward-looking orientation and attached to the same frames as the RBRduo^3 instruments. The ADCPs were programmed to collect velocity data every 10 min at 2 Hz for a burst of 60 samples (i.e. 30 s of data) in 0.03 m bins starting roughly 0.1 m above the seafloor from May through August 2021 and 2022. An approximately 30 cm diameter section of seagrass was removed surrounding the Aquadopp sensors to prevent interference with flow measurements. Using the internal instrument compass and tilt sensors, velocity measurements were recorded in the east-north-up coordinate system to produce both directional and horizontally averaged velocity profiles in 0.03 m bin elevations from z = 0.1 m to roughly z = 1.5 m (upper boundary due to instrument limit). Due to signal interactions with the water surface, velocities within 0.2 m of the water surface were not recorded. To determine the impacts of seagrass on mean flow structure, velocities at the top of the canopy (z = 0.3 m) were compared to velocities above the canopy (z = 0.6 m) as well as comparison at these 2 elevations from within and outside the canopy.

A Nortek Vectrino II acoustic Doppler velocimeter (ADV) was deployed along 2 transects at Site 1 to quantify changes in flow and turbulence conditions across various edges of vegetation. The longer edge transect covered 10 m, beginning 5 m away from the seagrass edge over a naturally bare seafloor, with the edge of vegetation as the transect midpoint, and continuing 5 m more into full vegetation past the edge. Velocity data was collected at 10 sampling locations in 1 m increments along the transect, which was located immediately west of the manmade bare patches. The shorter patch transect spanned 3 m, beginning in the center of the manmade bare patch (location C), crossing the edge of vegetation, and continuing 1.5 m into the seagrass. Data was collected at 7 sampling locations in 0.5 m increments along this transect. These distances were chosen to best quantify flow modification by the seagrass edge and patch over a time period during which tidal and wave conditions would not change appreciably from start to finish of a transect. At each transect sampling location, the Vectrino was attached to an immobile frame in a downward-facing orientation to record velocity data at an elevation of $z = 0.1$ m above the seafloor at 25 Hz for 5 min, resulting in 7500 samples at each location on the transects. If necessary, a small 10 cm diameter circular area of seagrass was removed to prevent interference with the Vectrino flow measurements. Four Vectrino transect deployments occurred, recording water velocities and H_s for each deployment shown in Table 1.

In summer 2022, 2 Nortek Vector ADV instruments were deployed at Site 2, located 10 m apart, each 5 m from the natural edge of seagrass vegetation at locations A and B. This distance was chosen to mimic the overall transect distance of the Vectrino data at Site 1. The vectors were placed facing downward on frames to collect data at $z = 0.1$ m. The instruments recorded data for 72 h per deployment, recording data every 20 min for a burst of 10 min duration at a sampling rate of 32 Hz.

Table 1. Average water velocities (cm s^{-1}) and significant wave height (H_s; cm) from the 4 Vectrino deployments along the 2 Site 1 transects during summer 2021. Water velocities and H_s were quantified at the beginning (unvegetated) and ending (vegetated) locations of each transect

	Velocity		H_s	
	(unvegetated)	(vegetated)	(unvegetated)	(vegetated)
15 July, Patch	5.7	1.4	4.4	3.7
26 July, Edge	6.2	1.4	3.2	5.0
10 Aug, Edge	13.3	1.8	<1.0	<1.0
18 Aug, Patch	4.4	2.0	<1.0	<1.0

Meteorological data were obtained from a nearby NOAA Station (WAHV2–8631044) in Wachapreague, VA, where wind speed (m s^{-1}) and direction were measured every 6 min.

2.3. Hydrodynamic data analysis

Both the Nortek Vectrino and Vector collect horizontal (u), transverse (v), and vertical velocities (w). Velocity components are separated due to their contributions to mean currents, turbulence, and waves by utilizing the phase method of spectral decomposition (Bricker & Monismith 2007). For example, u can be expressed as:

$$u = u' + \tilde{u} + \bar{u} \quad (1)$$

where u' is the turbulent velocity, $\tilde{u}$ is wave-induced orbital velocity, and $\bar{u}$ is the mean velocity. Following the decomposition methodology, $\bar{u}$ is first subtracted from the instantaneous velocities, and the power spectral densities (PSD) of the remaining fluctuating components of the velocities are computed. Larger values of spectral density correspond to a higher magnitude of energy in the flow for a given frequency, and integrating the area under the curve quantifies the magnitude. Generally, $0.3 < f < 2$ Hz encompass motions from the wave band and are identified within the spectra, then separated from that of mean flow and turbulence by quantifying a best-fit $-5/3$ slope line to the inertial subrange outside of the wave band (Hansen & Reidenbach 2012). Under spectral decomposition theory, spectral energy above the $-5/3$ inertial subrange fit is due to wave energy, while that below the fit is due to turbulent energy. This same technique is applied in the same way separately to the u, v, and w velocity components. This method of decomposition allows for the quantification of turbulent Reynolds stress (TRS) as:

$$\overline{u'w'} = \overline{uw} - \tilde{\bar{u}}\tilde{\bar{w}} \quad (2)$$

Further information regarding this method as applied in vegetated flows can be found in Hansen & Reidenbach (2012). Turbulent kinetic energy (TKE) is then quantified as:

$$\mathrm{TKE} = 0.5(\overline{u'^2} + \overline{v'^2} + \overline{w'^2} \quad (3)$$

Linear wave theory was used to quantify wave orbital velocities from water pressure data collected by the Vector's pressure sensor (Hansen & Reidenbach 2012). The spectral density of surface elevation, $S_{\eta\eta p,}$ is computed as:

$$S_{\eta\eta p} = \left[\frac{\cosh(kh)}{\cosh(kz)}\right]\frac{S_{pp}}{\rho^2 g^2} \quad (4)$$

where S_{pp} is the spectral density of the pressure, k is the wave number, h is the mean water depth, z is the height of the pressure sensor above the bottom, g is gravitational acceleration and ρ is density (Dean & Dalrymple 1991). H_s and average period (T) are then computed using the first ($m0$) and second ($m2$) moments from the $S_{\eta\eta p}$ power spectrum:

$$H_s = 4\sqrt{m0} \qquad T = \sqrt{m0/m2} \quad (5)$$

where $m0 = \int S_{\eta\eta p}(f)\mathrm{d}f$ and $m2 = \int f^2 S_{\eta\eta p}(f)\mathrm{d}f$. The horizontal component of orbital velocity, u_o, can then be computed as:

$$u_o = \frac{\pi H_s}{\sqrt{2}\,T}\frac{\cosh(kz)}{\sinh(kh)} \quad (6)$$

Assuming linear wave theory, the frequencies at or above which wave attenuation will occur at a given elevation z above the seafloor and in water depth h is given as (Wiberg & Sherwood 2008):

$$f > \sqrt{g/[4\pi(h-z)]} \quad (7)$$

All statistical analyses (ANOVAs, t-tests, correlation tests) performed on hydrodynamic data were conducted in R (version 4.2.2) (R Core Team 2022). Hydrodynamic calculations were conducted in Matlab (version R2021a).

2.4. Sediment sampling

The previously mentioned wave gauges (RBRduo^3) also contained turbidity sensors and were deployed in summer 2021 and 2022 for the same periods, from May through August 2021 and 2022, and at the same locations as the Aquadopp instrumentation. The sensors were programmed to measure in nephelometric turbidity units (NTUs) every 10 min at 4 Hz for a 1 min burst. In summer 2022, SSCs were also quantified using an optical backscatter sensor (OBS; Campbell Scientific OBS3+) connected to each Vector and housed on the same instrument frame to collect data concurrently. Values of NTU measured by the OBSs were converted to SSCs with units of mg l^{-1} using previously calculated calibration values (Hansen & Reidenbach 2012), performed on the same instruments and with sediment from the South Bay seagrass meadow.

Sediment traps were used to measure the deposition of sediment at Sites 1 and 2 (Fig. 2). The trap dimensions formed a 4:1 aspect ratio of internal length to internal diameter, which has been deemed appropriate for lower energy systems (Storlazzi et al. 2011). The trap designs were adapted from Wilson (1990) and constructed of 7.6 cm diameter PVC Charlotte piping, cut to a 30.5 cm length. Pipe caps (Charlotte) were used to seal the bottom ends of the traps, preventing sediment loss and allowing minimal water drainage. The traps were placed within PVC 'sleeves', which provided an easier method for frequent removal and replacement instead of continually redeploying into the sediment (Wilson 1990). Sleeves were made from PVC Charlotte Pipe of 10.2 cm diameter with a length of 28 cm. The sleeves were deployed into the sediment with an extension of 10 ± 2 cm above the seafloor, where they remained for the study period. This resulted in a final total trap height between 10 and 15 cm above the seafloor. To avoid faunal interference, a polypropylene mesh (6 mm mesh size) covered the opening of the trap. Considering the spacing guidelines described by Storlazzi et al. (2011), traps were deployed at Sites 1 and 2 where each transect location had 3 replicates spaced 1 m apart, yielding a total of 12 traps per deployment at Site 1 in 2021 at locations A–D (at the transect furthest to the north), and 9 traps at Site 2 in 2022 at locations A, B, and E. Traps were exchanged roughly every 2 wk. Trap contents were emptied into preweighed aluminum bins and any fauna collected were removed. The remaining sediment contents were dried at 60°C for at least 24 h and measured again for

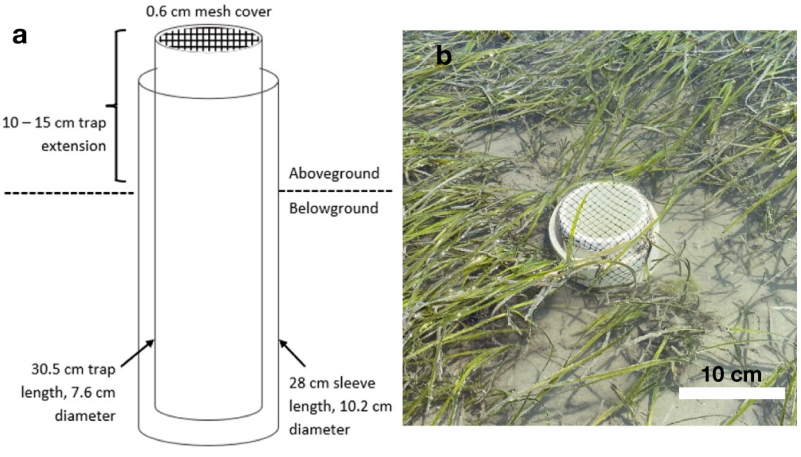

Fig. 2. (a) Schematic diagram of PVC sleeve and trap design adapted from Wilson (1990); not to scale. (b) Photo of sleeve and trap system deployed *in situ*

a final dry weight. This weight was divided by days of data collection and trap opening area to produce a total collection rate per area (g cm^{-2} d^{-1}). All statistical analyses (ANOVA, *t*-test, correlation tests) performed on sediment data were conducted in R (version 4.2.2) (R Core Team 2022).

2.5. Bivalve sampling

Sediment cores of 7.6 cm diameter were taken from the top 5 cm of sediment roughly every week from June through August 2021 at Site 1. Samples were taken at each of the 12 total locations (locations A–D) within a 3 m diameter adjacent to the sediment trap replicates. All contents were immediately bagged and placed on ice for transport to the laboratory, where they were refrigerated and then processed within 48 h of collection. All samples were wet-sieved through a 500 µm mesh, and remaining contents were examined without magnification and with a dissecting microscope. An identification key was used to distinguish ambiguous specimens and ensure that only bivalves were recorded, but specific species identifications were not performed. A 'count' in this methodology represents a bivalve between 500 µm and 1 cm in height with its hinge completely maintained and its valves almost entirely intact. Shell fragments or shell hinges with significant weathering were not counted. The final contents were preserved in 70% ethanol and frozen. Two additional rounds of samples were collected and processed in June 2022 at Site 1 to assess the consistency of results after the disturbance generated by creating the manmade bare traps and frequent sampling in summer 2021. A square-root transformation was applied to abundance values to meet assumptions of normality and perform statistical analyses. All statistical analyses (ANOVA, Tukey's tests) performed on bivalve data were conducted in R (version 4.2.2) (R Core Team 2022).

3. RESULTS

3.1. Physical conditions

During summer 2021 at Site 1 (mean density: 555 ± 75 shoots m^{-2}), average water depth, as computed from wave gauges, was 1.5 m with tidal fluctuations, resulting in minimum and maximum depths of 0.4 and 3.0 m, respectively. During summer 2022 at Site 2 (mean density: 200 ± 50 shoots m^{-2}), average depths at the seagrass site were 1.2 m, with minimum depths close to zero during extreme low tides and maximum depths exceeding 2 m. Average monthly wind speeds during summer 2021 ranged from 2.5 ± 0.1 to 4.2 ± 0.1 m s^{-1}, with monthly averaged H_s at Site 1 within both the bare and seagrass locations ranging from 0.05 to 0.10 m. H_s did not differ significantly between the 2 locations over the entire study period (1-way ANOVA, $F_{1,6} = 0.012$, $p = 0.916$). Maximum H_s (0.6 m) occurred during a storm in late May 2021, leading to significantly higher H_s averages for the month overall (1-way ANOVA, $F_{3,4} = 274.6$, $p < 0.001$). Average wind speed during summer 2022 ranged from 3.4 to 4.7 m s^{-1}, with average monthly H_s of 0.07 m and a maximum during a storm (18–20 June 2022) with heights exceeding 0.3 m.

3.2. Mean flow conditions

To address differences in current flow over longer durations of the study period in different sampling locations and across changes in vegetation density, mean velocities throughout the water column were quantified concurrently across Site 1 in seagrass vegetation and along the adjacent bare seafloor. Mean velocities at canopy height (z = 30 cm) ranged from 2.5 to 5.1 cm s^{-1} in seagrass vegetation and from 6.8 to 9.1 cm s^{-1} over the unvegetated seafloor (Fig. 3). Mean velocities in seagrass vegetation were statistically significantly (ANOVA, $F_{1,8} = 42.45$, $p < 0.001$) lower than in adjacent bare areas, with reductions between the 2 sites ranging from 40 to over 60%. In general, tidal flows and wave propagation followed a roughly north–south orientation, creating flows that were parallel to the seagrass edge. There were also statistically significant reductions in velocity at each sampling site, comparing elevations of z = 60 cm (above canopy height) to 30 cm [$100 \times (\bar{u}_{z=0.6m} - \bar{u}_{z=0.3m})/\bar{u}_{z=0.6m}$], with seagrass site having up to a 35% decrease in water velocity at the lower elevation (ANOVA, $F_{1,10} = 5.726$, $p = 0.038$), whereas the bare site only experienced up to a 20% decrease (ANOVA, $F_{1,8} = 8.563$, $p = 0.019$) (Fig. 3). Seagrass density peaked in July and corresponded with the season's lowest measured mean velocities of 3.5 cm s^{-1} at canopy height (z = 30 cm).

3.3. Hydrodynamic conditions across edges

In summer 2021, a Vectrino was used to quantify velocities along 2 transects at Site 1: a 10 m transect crossing the natural edge of vegetation and a 3 m

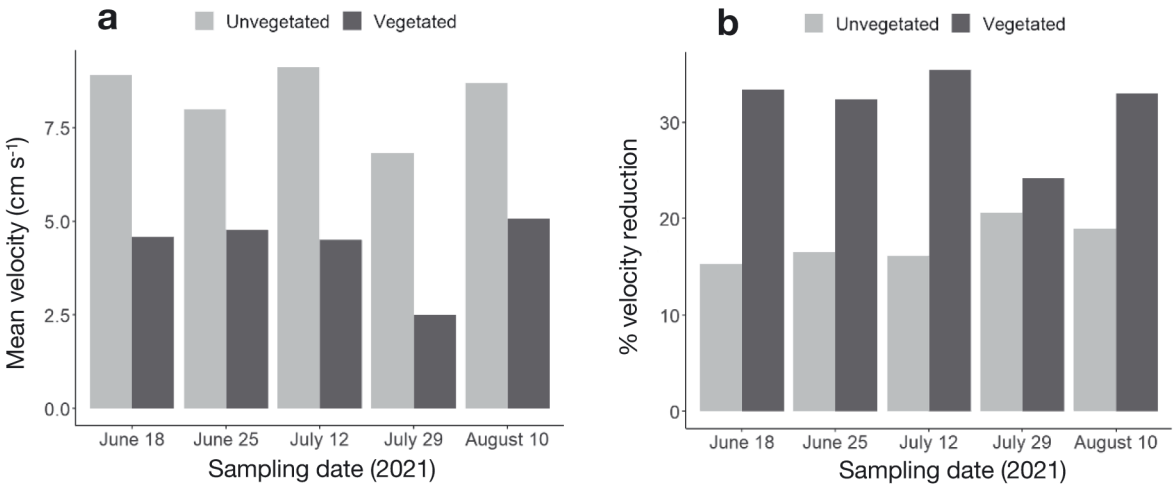

Fig. 3. (a) Mean velocities quantified at a z = 30 cm elevation above the seafloor for each deployment period of 2021 from unvegetated (light) and vegetated (dark) sampling locations. (b) Percent velocity reduction from z = 60–0 cm elevations in the water column [$100 \times (\bar{u}_{z=0.6\mathrm{m}} - \bar{u}_{z=0.3\mathrm{m}}) / \bar{u}_{z=0.6\mathrm{m}}$], at vegetated and unvegetated sampling locations

transect covering the manmade bare patch. Data were collected at an elevation of z = 0.1 m in 1 m increments along the edge transect and in 0.5 m increments over the patch transect for 5 min in each sampling location. Values were averaged into a representative mean for each sampling increment, including velocity magnitude, TRS, and power spectra, showing the magnitude of energy in the flow at different frequencies. A representative profile of mean velocity and TRS from the patch transect is shown in Fig. 4 along with the corresponding PSD from unvegetated and vegetated sampling locations along that transect. Mean velocities were reduced in seagrass by 50–75% (Fig. 4). Flow energy and associated reductions in vegetation at different frequencies are visualized with PSDs, which depict energy magnitude at corresponding frequencies. At almost all frequencies, flow energy in bare areas exceeded that of flows within the vegetation. However, energy from frequencies in the wave band ($0.3 < f < 2$ Hz) were similar in both sampling locations, suggesting that low-frequency oscillatory wave energy from wind-generated waves penetrates the seagrass canopy and reaches similar magnitude close to the seafloor. Two velocity profiles from the 10 m long edge transect are shown in Fig. 5, indicating reductions of mean flow in vegetated areas that exceeded 80% compared to the unvegetated site. Average H_s during both transects was 0.05 m. Overall, mean velocities within the constructed bare patch were lower than those over naturally bare seafloor during the same period of data collection, with similar flow and wave conditions.

During summer 2022, 2 Nortek Vector ADVs were concurrently deployed in a stationary (non-profiling) orientation at Site 2, 3 separate times for a minimum of 72 h. The instruments were placed 10 m apart, spaced evenly across the natural edge of meadow vegetation. Each of the 3 deployments was characterized by different physical conditions. Deployment 1 (13–16 May) had the lowest seagrass densities (150 ± 40 shoots m^{-2}) and low–medium wave activity, Deployment 2 (23–26 May) had statistically similar low seagrass densities but the greatest wave activity, and Deployment 3 (10–13 June) had the highest seagrass densities (245 ± 50 shoots m^{-2}) and lowest wave activity. These combinations of meadow morphologies and physical settings allowed analysis of how velocity, turbulence, waves, and sediment resuspension respond to different conditions in bare and vegetated areas immediately surrounding a seagrass edge.

Depth and H_s data for each deployment are shown in Table 2. Mean velocities at the unvegetated site ranged from 8.8 to 11.1 cm s^{-1} and from 3.3 to 7.7 cm s^{-1} at the vegetated site. This variability was primarily due to tidal currents. Mean velocities were highest during Deployment 1 and decreased with each subsequent deployment, displaying an inverse relationship with seagrass shoot density. Mean velocities were consistently and significantly higher in magnitude at the unvegetated location (2-sided t-test, t_4 = 3.12, p = 0.036). Percent reduction of mean flow speed between the 2 sampling locations ranged from 30% during Deployment 1 to over 65% during Deployment 3, correlating with increases in seagrass shoot density.

TRS was significantly greater in magnitude (Fig. 6) at vegetated locations (2-sided t-test, t_4 = −4.55, p =

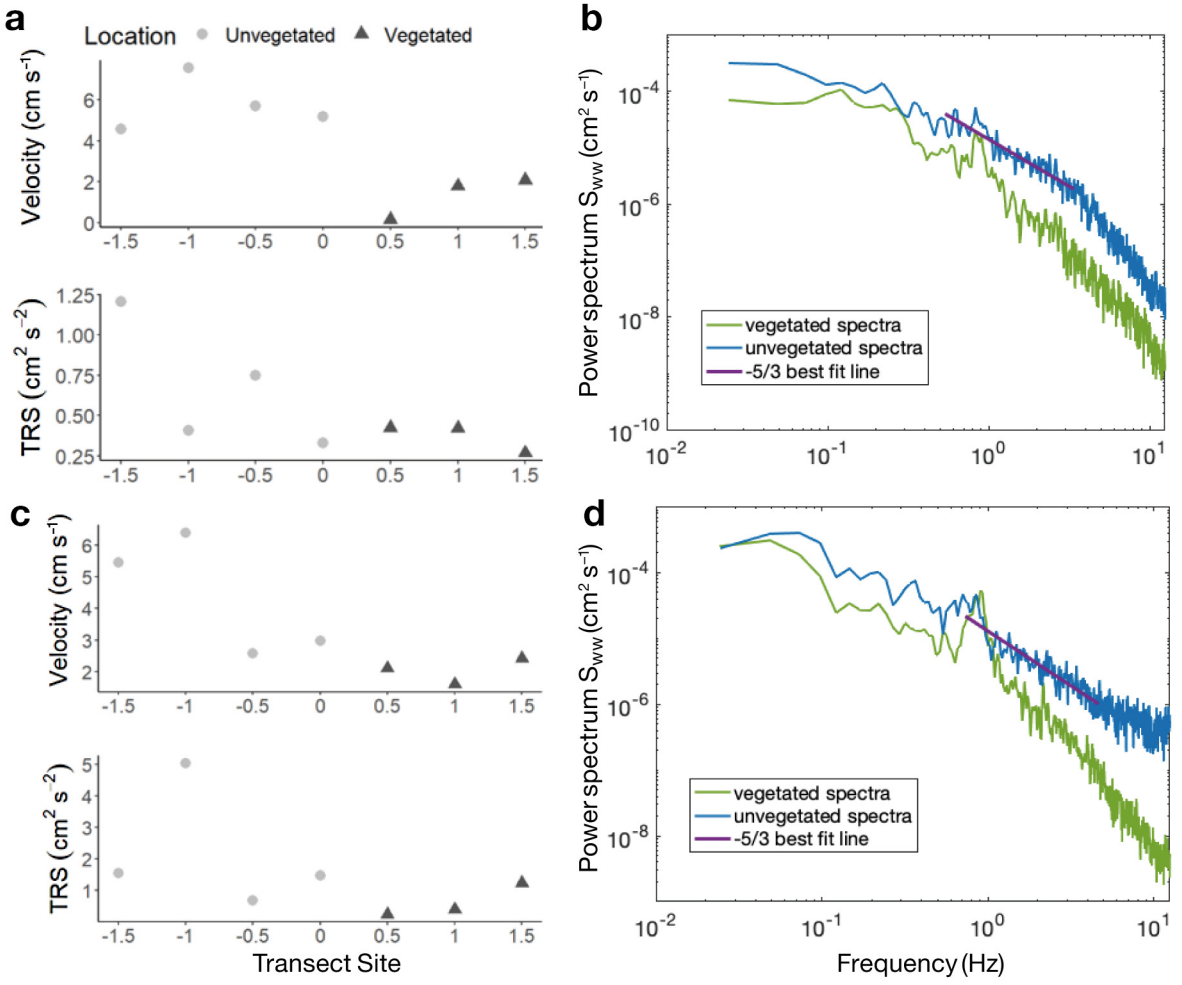

Fig. 4. Profiles of mean velocity and turbulent Reynolds stress (TRS) at z = 0.1 m from transects spanning the manmade bare patch on (a) 15 July 2021 and (c) 18 August 2021, and (b,d) power spectral densities of the vertical velocity, S_{ww}, from the same dates quantified in unvegetated and vegetated sampling locations. The −5/3 slope lines shown in each graph indicate the best fit to the inertial subrange of the turbulence. Significant wave heights during both sampling times were ~0.05 m. Distance between transect sites is 0.5 m and seagrass edge begins between Sites 4 and 5. Mean wind and flow conditions for the transects shown are included in Table 1

0.011), ranging from 0.29 to 0.36 cm^2 s^{-2} at the bare site and from 0.49 to 0.75 cm^2 s^{-2} in the vegetated site. Wave orbital velocities were quantified at the 2 sites and ranged between 3.1 and 17.3 cm s^{-1}. There were no significant differences in average magnitude between the 2 sampling locations during each deployment, as indicated by similar H_s between sampling locations. The similarity in wave orbital velocities between sampling locations is also consistent with the similarity in energy from frequencies in the wave band ($0.3 < f < 2$ Hz) shown in PSDs. Deployment 2 experienced the greatest wave activity, caused by elevated wind speeds during this time resulting in the upper limit of measured wave orbital velocities (17 cm s^{-1}). Orbital velocities measured during Deployments 1 and 3 ranged, on average, between 3 and 4 cm s^{-1} and more closely resembled mean flows measured over the duration of the study period.

PSDs of vertical velocities measured concurrently at bare and vegetated sites indicate that flows were dominated by tidal current during Deployment 1 and by wave activity during Deployment 2 (Fig. 7). During tidally dominated flow conditions, a distinct −5/3 slope exists in the spectra across 0.2–6 Hz frequencies of motion, indicating an expected inertial subrange. Energy magnitude across these frequencies was generally similar between the unvegetated and vegetated sampling locations in this example. During wave-dominated conditions, oscillatory flow due to wave activity adds energy to the turbulent flow and creates a distinctive peak in the PSD across the wave band ($0.3 < f < 2$ Hz), disrupting the characteristic −5/3 slope of the PSD characterizing the inertial

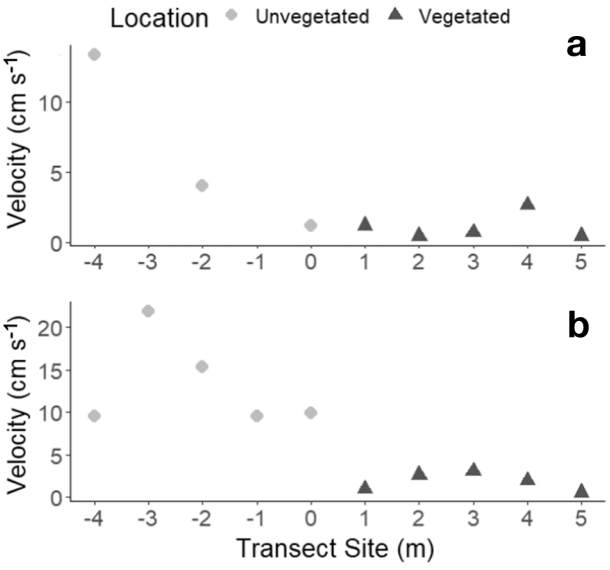

Fig. 5. Profiles of mean velocity at z = 0.1 m from transects spanning the meadow's natural edge of vegetation on (a) 26 July 2021 and (b) 10 August 2021. Distance between transect sites is 1 m, and the meadow edge begins at 0 m. Mean wind and flow conditions for the transects shown are included in Table 1. Due to instrument error, no data was collected at transect site −4 or −2 m on 26 July 2021

subrange in this region. Outside of the frequencies encompassing the wave band, the same −5/3 trend exists. Wave motion effectively penetrated the seagrass canopy, similar to the unvegetated region, as evident by the distinctive peak in the wave frequency band ($0.3 < f < 2$ Hz).

PSDs showing horizontal and vertical velocities for frequencies from 0 to 2 Hz from the bare and vegetated locations are shown for the higher wave conditions during Deployment 2 (Fig. 8). The black line oscillating across the PSDs portrays the frequency threshold at or above which wave attenuation may be expected due to natural decay of the waves with depth under linear wave theory (Eq. 7). Gaps in data are due to low water levels at low tides leaving the sensors exposed. The data suggest minimal attenuation of wave frequencies ($0.3 < f < 2$ Hz) in vegetated locations even at relatively high wave activity but a reduction in low frequencies of $f < 0.3$ Hz in vegetated locations, thus reflecting a reduction in larger, slower turbulent overturns due to drag imposed by the seagrass. It is these lower frequencies ($f < 0.3$ Hz) that contribute the majority of the energy to the bulk flow.

Table 2. Average and maximum water depth (±1 SE, m) and significant wave height, H_s (±1 SD, m), from the unvegetated and vegetated sampling locations of the 3 Vector deployments at Site 2 during summer 2022. Water depths were statistically different between unvegetated and vegetated sites within a given deployment, but H_s was not statistically different

	Deployment 1: 13–16 May		Deployment 2: 23–26 May		Deployment 3: 10–13 June	
	Unvegetated	Vegetated	Unvegetated	Vegetated	Unvegetated	Vegetated
Avg. depth	1.04 ± 0.014	0.90 ± 0.014	1.20 ± 0.007	1.09 ± 0.007	0.97 ± 0.007	0.89 ± 0.007
Max. depth	1.95	1.78	1.92	1.83	1.86	1.78
Avg. H_s	0.06 ± 0.06	0.06 ± 0.06	0.14 ± 0.08	0.16 ± 0.08	0.04 ± 0.04	0.05 ± 0.04
Max. H_s	0.14	0.16	0.32	0.32	0.09	0.11

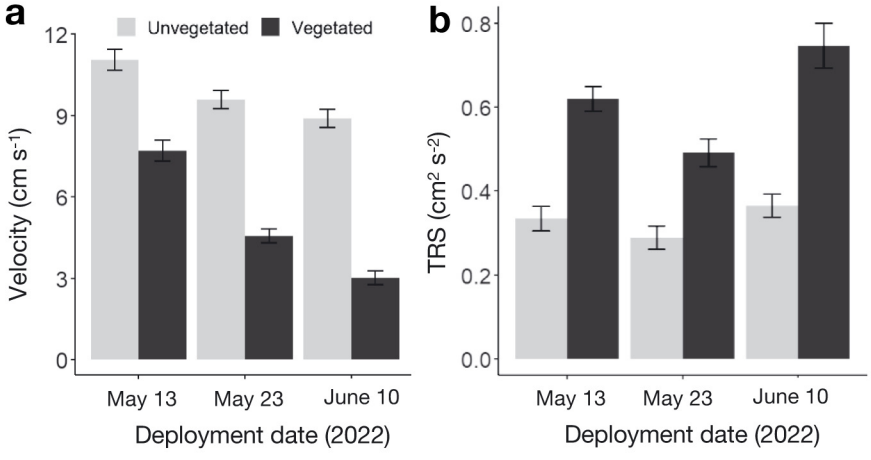

Fig. 6. Mean (±SE) (a) velocities and (b) turbulent Reynolds stresses (TRS) shown from unvegetated and vegetated sampling locations during the 3 Vector deployments in 2022 (13 and 23 May and 10 June 2022)

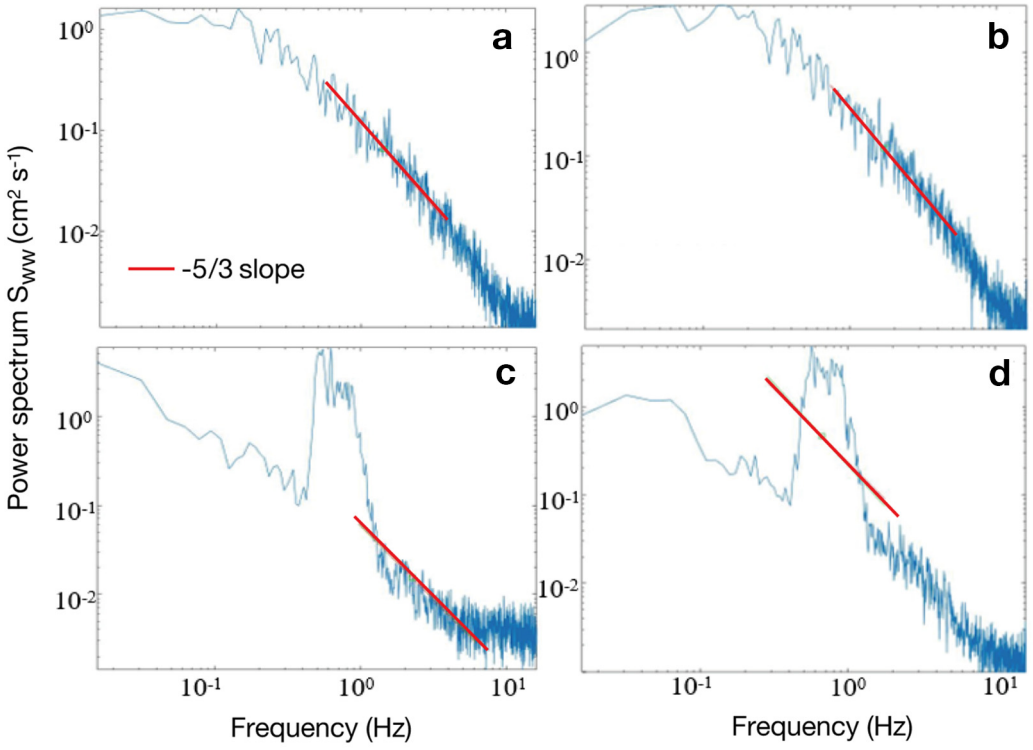

Fig. 7. Power spectral densities of vertical velocity energy magnitude at various frequencies from (a,c) unvegetated and (b,d) vegetated sampling locations. Deployment 1 of summer 2022 is shown in (a) and (b) with current-dominated conditions and Deployment 2 is shown in (c) and (d) with wave-dominated conditions. The −5/3 slope lines indicates the inertial subrange of turbulence in (a) and (b); in (c) and (d), the addition of wave energy within the wave frequencies ($0.3 < f < 2$ Hz) disrupts the characteristic −5/3 inertial subrange

3.4. Sediment suspension and deposition

Sediment accumulation rates from all sediment trap collections in 2021 are shown in Table 3. Variability between sampling locations remained high, but the rates were statistically similar, with sediment accumulation rates averaged across all sampling dates ranging from 0.56 to 0.74 g cm^{-2} d^{-1}. The first round of deployments from 25 May to 2 June had sediment collection rates nearly 10 times higher than other periods, likely due to a large storm. To limit variability from this outlier, the spatial groupings were analyzed again, excluding the first round of collection. These averages for locations A–D were 0.26, 0.28, 0.37, and 0.27 g cm^{-2} d^{-1}, respectively (Table 3), which showed lower mean values but similar trends in deposition when comparing sampling locations. SSCs (in NTU), wind speeds, and H_s were concurrently measured at Site 1, and no significant differences between these values based on their location in bare or vegetated seafloor were found. SSC values were then grouped by month regardless of sampling location to address seasonal changes, and the

Table 3. Sediment trap accumulation rates (g cm^{-2} d^{-1}) from 2021 at Site 1 where the 3 replicates from each sampling location (A–D) are averaged into one value for that round of data collection. Bottom 2 rows show the total mean (±1 SE) of that sampling location over the study period, both including and excluding the elevated first round of trap collection (Rd1) in late May. Location A: the unvegetated seafloor 5 m from seagrass edge; location B: 5 m from the edge, within the seagrass meadow; location C: a manmade bare patch 15 m from the edge; location D: 25 m from the edge within the meadow

Collection dates (2021)	A	B	C	D
25 May–2 June	2.86	2.61	2.73	2.03
2–16 June	0.32	0.17	0.35	0.25
18–29 June	0.36	0.32	0.28	0.18
29 June–10 July	0.21	0.20	0.26	0.23
27 July–9 Aug	0.12	0.22	0.21	0.19
9 Aug–10 Sept	0.13	0.19	0.44	0.19
10 Sept–12 Oct	0.44	0.65	0.66	0.59
Mean incl. Rd1	0.67 ± 0.24	0.65 ± 0.2	0.74 ± 0.22	0.56 ± 0.16
Mean excl. Rd1	0.26 ± 0.05	0.28 ± 0.08	0.37 ± 0.07	0.27 ± 0.07

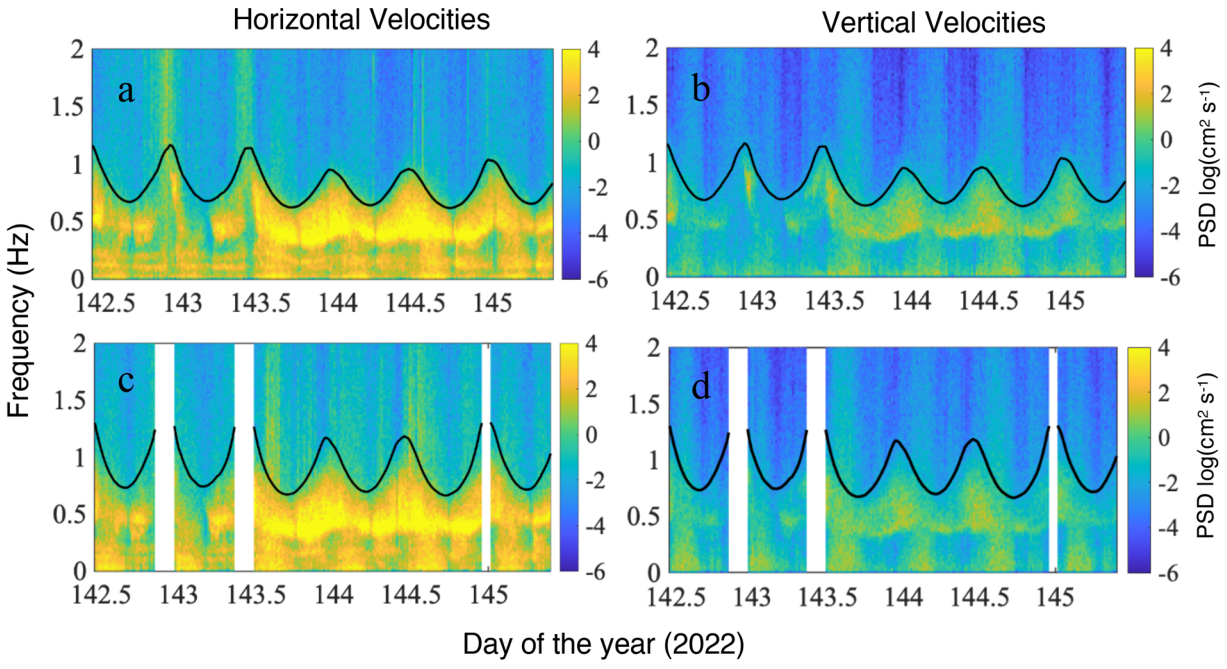

Fig. 8. Power spectral density (PSD) of (a) horizontal and (b) vertical velocities at frequencies under 2 Hz at the unvegetated location and (c) horizontal and (d) vertical velocities at the vegetated location during Vector deployment 2 at Site 2. Black lines: the lower threshold of expected wave attenuation, which is inversely related to the square root of the water depth. Gaps in the figure represent periods of no data collection due to instrument exposure at low tide

resulting means are shown in Fig. 9; like trap collection rates, SSC was elevated in May. Wind speed and wave heights were also elevated and reached their seasonal maximums in late May due to a storm (Pearson correlation tests between NTU and trap collection rate: $r^2 = 0.986$, $p = 0.014$; NTU and H_s: $r^2 = 0.988$, $p = 0.012$; trap collection rate and H_s: $r^2 = 0.958$, $p = 0.042$). Overall, elevated SSC correlated with higher wind speeds, which tended to produce larger wind-driven wave heights as evident during the May 2021 storm (Fig. 10).

Rates from all rounds of collection at Site 2 during 2022 are shown in Table 4, where mean rates for locations A, B, and E were 0.2 ± 0.02, 0.29 ± 0.06, and 0.15 ± 0.02 g cm^{-2} d^{-1}, respectively, similar to collection rates from 2021. Location B (vegetated location

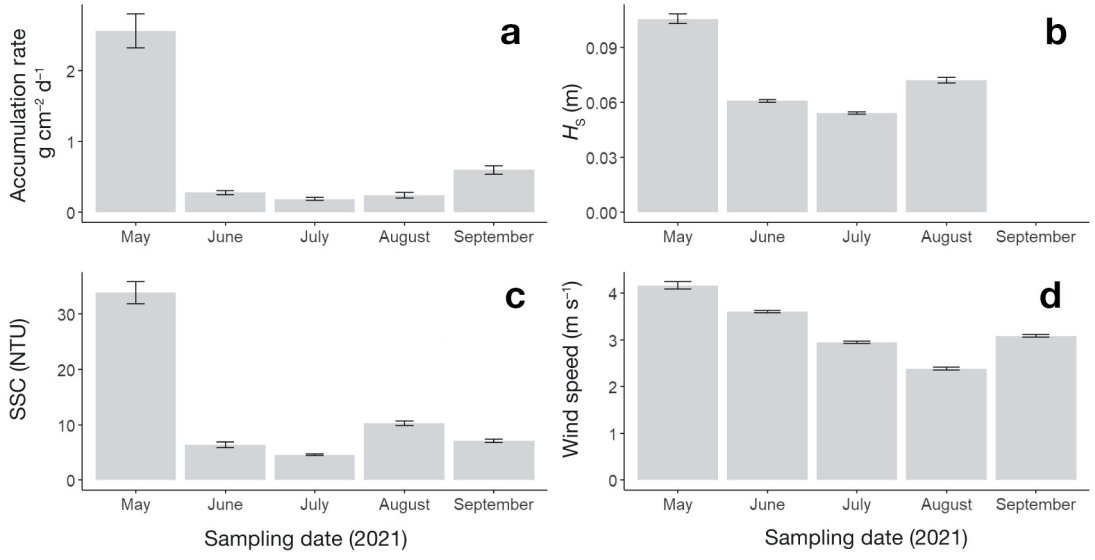

Fig. 9. Monthly averages (±1 SE) of (a) sediment accumulation rate, (b) significant wave height (H_s), (c) suspended sediment concentration (SSC), and (d) wind speed from Site 1 during 2021

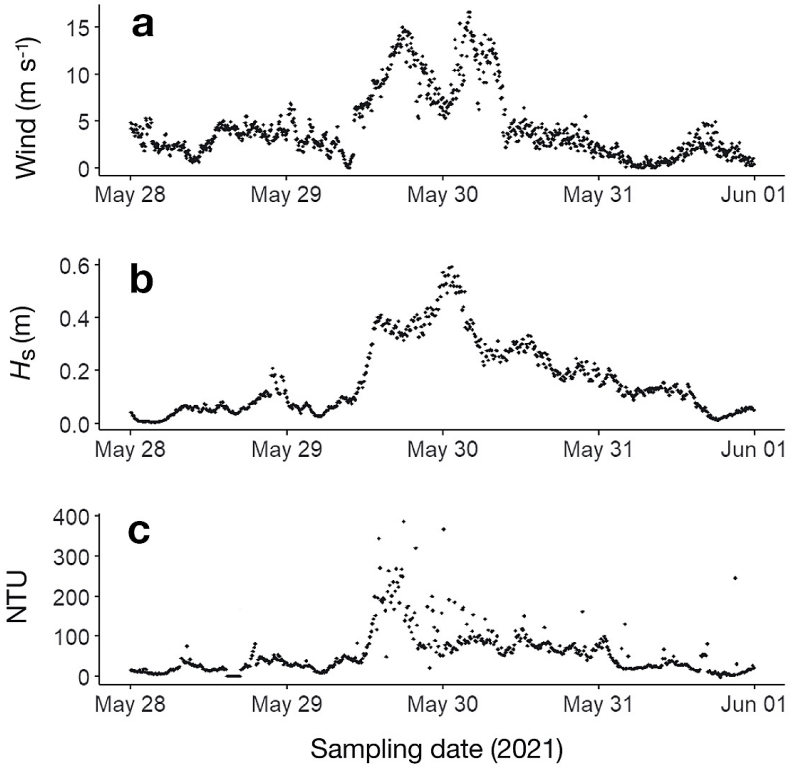

Fig. 10. Time series data of (a) wind speed, (b) significant wave height, H_s, and (c) turbidity (NTU) from the vegetated sampling location at Site 1 during a storm from 28 May–1 June 2021

closest to natural edge) had elevated collection rates but was statistically similar to location A (in the unvegetated region), while location E (100 m into vegetation away from meadow's edge), had a nearly significant lower collection rate (2-sided *t*-test, t_{12} = 2.11, p = 0.056). To further address sediment movement across seagrass edges, sediment sensors were deployed at Site 2 in 2022 to measure SSCs in the water column at locations A and B, spanning the meadow's natural edge of vegetation. Fig. 11 shows the resulting average SSCs with average values between 54 and 106 mg l^{-1}. Consistent with trap collection data, SSCs were similar to or slightly higher within the vegetated sampling locations 5 m within the seagrass meadow compared to 5 m outside the seagrass meadow. This elevated SSC corresponds to increased TRS measured within the vegetation compared to outside the vegetation. This suggests that the low canopy density (average of 200 ± 50 shoots m^{-2} for summer 2022) can locally increase near-bed turbulence and SSC concentrations compared to higher canopy densities measured during summer 2021 (average of 555 ± 75 shoots m^{-2}).

3.5. Bivalve recruitment

Abundances from all rounds of core sampling during 2021 are shown in Fig. 12. A 1-way ANOVA and Tukey's test were performed to address differences between core abundances at the 4 different sampling locations over the entire study period. The locations were statistically different (ANOVA, $F_{3,103}$ = 22.27, p < 0.0001), except between locations B and D, indicating that bivalve abundances were lowest in naturally bare areas (location A), elevated in the artificial bare patch within the seagrass bed (location C), and greatest in

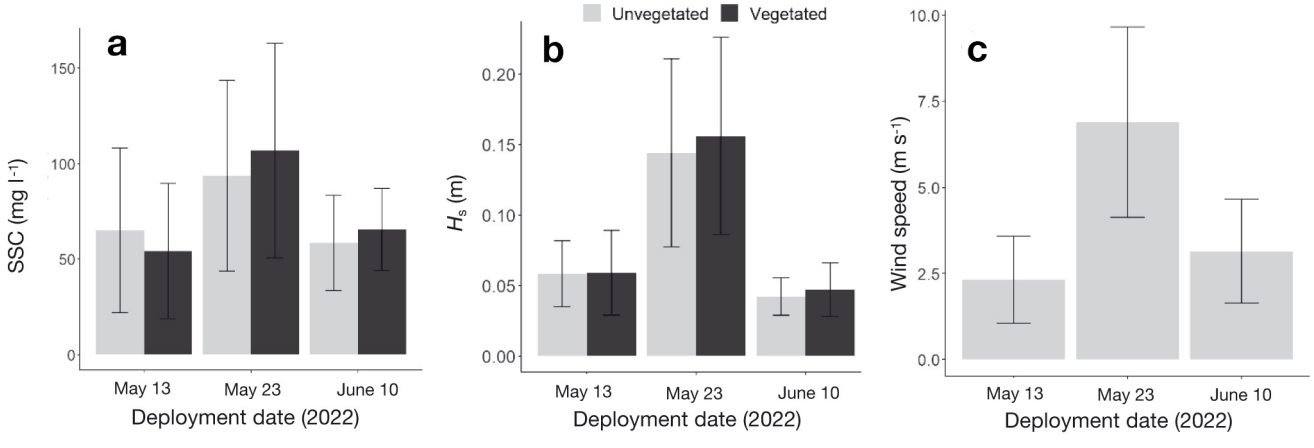

Fig. 11. Averages (±1 SD) of (a) suspended sediment concentration (SSC), (b) significant wave height (H_s), and (c) wind speed from periods of Vector deployment at Site 2 during summer 2022

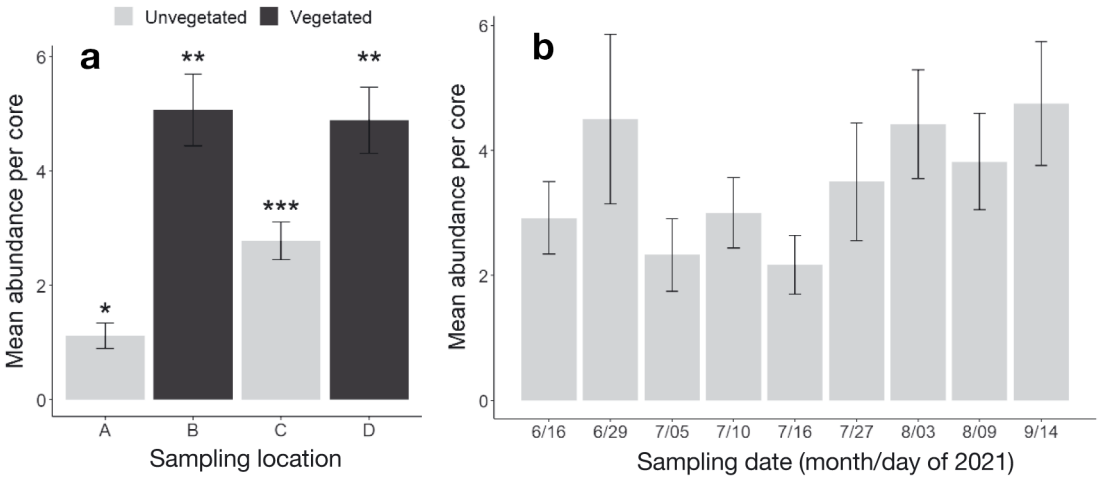

Fig. 12. (a) Mean (±1 SE) abundances of bivalves per core (core volume = 1390 cm^3) from each sampling location (locations A–D) averaged over the entire study period of 2021. Location A: naturally bare seafloor; location C: artificial bare patch; locations B and D: vegetation 5 and 25 m past the meadow's natural edge, respectively. Values with a different number of ⋆ denote a significant difference (1-way ANOVA, $p < 0.001$). (b) Mean abundances (±1 SE) of bivalves per core at all sampling locations from each round of collection (month/day) during summer 2021. A square-root transformation was applied to abundance values to meet assumptions of normality

Table 4. Sediment trap accumulation rates (g cm^{-2} d^{-1}) from 2022 at Site 2 where the 3 replicates from each sampling location (A, B, and E) are averaged (±1 SE) into one value for that round of data collection. Location A: the unvegetated seafloor 5 m from seagrass edge; location B: 5 m from the edge within the seagrass meadow; location E: 100 m from the edge within the meadow

Collection dates (2022)	A	B	E
13–26 May	0.28	0.43	0.18
26 May–10 June	0.13	0.14	0.08
10–30 June	0.19	0.37	0.17
Mean	0.20 ± 0.02	0.29 ± 0.06	0.15 ± 0.0

areas of full vegetation regardless of edge proximity (locations B and D). Compared to naturally bare location A, mean abundances were over 2.5 times greater in location C and over 4 times greater in locations B and D. A separate 1-way ANOVA was performed to address temporal variation with all the locations grouped (Fig. 12B). There was high temporal variability with no significant differences in abundance found between June and Sept (ANOVA, $F_{8,98} = 0.992$, $p = 0.447$).

During summer 2022, core samples were collected and processed in the same way at Site 1. The removal sites were not cleared again, so 2022 samples from location C reflect a year of re-growth, but these locations were still roughly 80% unvegetated. The resulting spatial averages from sampling locations A–D were 1.5, 5.7, 3.2, and 4.7 individuals per core, respectively, statistically similar to those from summer 2021 (Fig. 13).

4. DISCUSSION

4.1. Hydrodynamics

Wind speeds and significant wave heights were closely correlated (as shown in Fig. 10), with recorded increases in wind leading to greater H_s and wave orbital velocities. Despite this strong positive relationship

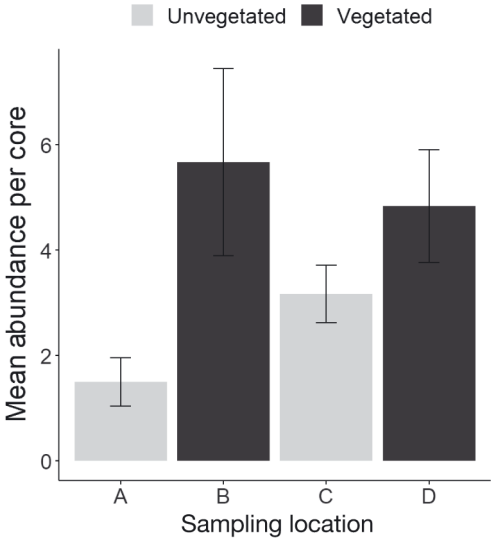

Fig. 13. Mean abundances (±1 SE) of bivalves per core (core volume = 1390 cm^3) from each sampling location averaged over the entire study period of 2022 at Site 1. Location A: naturally bare seafloor; location C: artificial bare patch; locations B and D: vegetation 5 and 25 m past the meadow's natural edge, respectively

between winds and waves, there was no statistical evidence of wave attenuation in seagrass vegetation compared to measurements taken in the adjacent, naturally bare seafloor. The lack of measurable wave attenuation across this 10 m distance (Table 1) differs from previous research that showed measurable attenuation of wave activity over longer spatial distances, with a total decrease of 30% across a 39 m transect of continuous seagrass bed (Bradley & Houser 2009). However, previous work has also shown that unlike unidirectional flow, wave attenuation is not abrupt (Infantes et al. 2012) but may initially increase in significant wave height as waves enter the seagrass bed and subsequently decrease exponentially over the remainder of the bed (Bradley & Houser 2009). Overall, there is an exponential decay rate that can vary in response to seagrass density and geometry, with wave attenuation increasing as the wave orbital excursion length is increased (Lowe et al. 2005). Longer-period wave motions (including those at tidal periods) can be significantly more attenuated than shorter-period oscillatory motions (Lowe et al. 2007). For the wave heights produced in this study, wave orbital velocities were able to effectively penetrate the seagrass meadow, both at the high seagrass density Site 1 and the low seagrass density Site 2, altering flow dynamics at the seafloor. Our results also indicated that greater flow reduction occurred with increased seagrass blade densities, agreeing with previous research that canopy presence and blade density are responsible for mediating the magnitude of current flow attenuation (Koch & Gust 1999, Peterson et al. 2004).

Turbulence regimes at Site 1 showed generally reduced total Reynolds stresses in seagrass vegetation, but these measurements coincided with high vegetation densities (>500 shoots m^{-2}). Results from summer 2022 reveal opposite trends, with greater Reynolds stresses 5 m into the seagrass vegetation within low-density regions of the seagrass canopy (<250 shoots m^{-2}). This finding aligns with findings from Hansen & Reidenbach (2012) that turbulent energies can be elevated in vegetated areas of low shoot density due to increased stem–wake interactions in a lower-density canopy (Widdows et al. 2008). This increase in turbulence was also reflected in PSDs from the low shoot density Site 2, which showed elevated magnitudes of turbulent energy in seagrass within turbulence frequencies (>3 Hz) of the energy spectra. Measured PSDs at both sites indicate the concurrent decrease in energy at low frequencies (<0.3 Hz), reflecting a reduction in mean flow. All PSDs revealed similar wave orbital velocities ($0.3 < f < 2$ Hz) within seagrass vegetation compared to unvegetated regions across the seagrass edge, suggesting that waves effectively penetrate the seagrass canopy that can impact flow interaction with the seabed.

4.2. Sediment dynamics

Sediment trap collection rates and SSCs were significantly correlated with each other and with H_s. Winds have previously been shown to be the dominant control of wave activity in this system (Fagherazzi & Wiberg 2009). Wave height was a major predictor of sediment resuspension and transport across these edge settings, and although benthic microalgal concentrations have been shown to impact resuspension rates (Reidenbach & Timmerman 2019), similar wave heights in these locations explain similar levels of sediment movement. Since the average grain size diameter is small at $D_{84} < 160$ µm (where D_{84} is the sediment grain diameter such that 84% of grain diameters are smaller), once suspended, sediments typically remain in suspension for a few days (Hansen & Reidenbach 2012). Sediment trap collection rates at Sites 1 and 2 showed no significant spatial trends across sampling locations within 25 m of the seagrass edge, whether in bare or vegetated areas or manmade removal areas. However, more notable reductions in sediment deposition occurred 100 m from the edge (measured at Site 2). This agrees with the work of Zhu et al. (2021, 2022), who concluded that vegetation density mediates the response of flow along seagrass edges, which creates lower sediment deposition rates along the interior of the meadow relative to deposition rates within ~100 m of edges. Within 25 m of the seagrass edge, high variability from trap collection data could explain the statistical similarities in these results, but high-resolution, longer-term data sets from optical backscatter sensors were used to concurrently quantify relative levels of SSCs and confirmed nonsignificant differences in turbidity. This suggests that as seen with wave attenuation (Verduin & Backhaus 2000), a threshold of distance from the meadow's edge may exist for vegetation to reduce SSCs (Zhu et al. 2022) but is likely greater than the ~25 m from the edge measured in this study.

4.3. Bivalve recruitment dynamics

Abundances of juvenile bivalves were elevated in all vegetated sampling locations regardless of proximity to edges. Abundances were lower in manmade bare

patches and lowest in naturally unvegetated seafloor. These results indicate that seagrass biomass enhances settlement and/or retainment of juvenile bivalves and is consistent with work showing greater bivalve presence in seagrass ecosystems (Orth et al. 1984, Glaspie & Seitz 2017). However, seagrass locations with elevated bivalve abundances also correspond to areas with significant reductions in mean flow. This suggests that the magnitude of the current flow (due to the combined effects of waves and tidal-driven flows) may still mediate bivalve settlement across vegetated locations (Bologna & Heck 2000) and that lower energy flow conditions encourage greater recruitment. The enhanced recruitment, therefore, may be due to the benefits of a reduction in flow forces imposed on settling larvae (Reidenbach et al. 2009, 2021) and decreased mortality and predation (Orth et al. 1984, Boström et al. 2010) through sheltering by the seagrass canopy. Previous research has shown significant wave attenuation at more interior locations of the seagrass bed (Reidenbach & Thomas 2018), which may also impact bivalve recruitment. However, along the edges of seagrass measured in this study, no significant changes in wave oscillations were measured within and outside the meadow, so the effects of waves on bivalve recruitment could not be determined.

Of note is the strong impact that seagrass edges have on bivalve recruitment but a much weaker response to sediment deposition dynamics. This may be due to the more active swimming behaviors of some settling larvae, which can alter settlement locations to a much greater degree (Abelson & Denny 1997, Koehl & Reidenbach 2007) than passive sediment particles. However, this direct effect of larval behaviors on settlement dynamics within seagrass systems has not been studied.

4.4. Conclusions

The results presented here indicate that over various edges of heterogenous vegetation along different spatial configurations, mean velocities were consistently and significantly reduced in seagrass vegetation and negatively correlated with increased shoot density. However, over these short spatial distances of <10 m, there was no evidence of wave attenuation or within-canopy wave orbital velocities in any of the vegetated locations. Interestingly, along edges of vegetation, total Reynolds stresses were elevated in seagrass vegetation in low-density regions, indicating a higher level of turbulent energy, presumably due to increased stem–wake interactions (Nepf et al. 1997, Widdows et al. 2008), the magnitude of which depends upon the flexibility of the blades and whether the vegetation is emergent or submerged. Although these findings generally agree with previous laboratory and field measurements of wave attenuation and turbulence (Bradley & Houser 2009, Infantes et al. 2012) for submerged and flexible vegetation, our study addressed how these changes impact sediment and bivalve settlement.

Our findings suggest that unlike wave motions, abundances of juvenile bivalves respond rapidly over short spatial distances of <10 m, with abundances of juvenile bivalves being significantly elevated in seagrass vegetation, presumably due to the sheltering effect caused by seagrass. However, there were no significant changes in turbidity or sediment collection rate at locations within 25 m of the meadow edge, but reduced collection rates were found at 100 m distances. This agrees with previous literature demonstrating reduced SSCs in vegetation across larger spatial scales (Carr et al. 2010, Hansen & Reidenbach 2013). Recent modeling work from South Bay reports that SSCs fluctuate non-linearly as a function of seagrass density and that meadow edges experience the greatest sensitivity to seasonal erosion or deposition due to either mean flows or wave activity while mediating overall advection of SSCs at the meadow scale (Zhu et al. 2022). Flume experiments showed a similar density-dependent relationship between flow regime and distance of sediment deposition past a seagrass edge (Zhang & Nepf 2019). This emphasizes that a minimum threshold of density and/or distance from a meadow's edge may exist to attenuate waves, thus causing a reduction in SSC and sediment deposition, and our findings suggest this distance to be on the scale of 100 m. However, in regions of low wave activity where tidal currents dominate, seagrasses are more effective at reducing flow energy, and this distance over which sediment transport is altered should be significantly reduced.

Data availability. Data are accessible at https://doi.org/10.6073/pasta/30de0c4d1086cd7ecb643f5b05c88d8b.

Acknowledgements. We thank the staff at the Anheuser-Busch Coastal Research Center for assistance in field campaigns. This research was funded by the National Science Foundation grant DEB-1832221 to the Virginia Coast Reserve Long Term Ecological Research project.

LITERATURE CITED

Abelson A, Denny MW (1997) Settlement of marine organisms in flow. Annu Rev Ecol Syst 28:317–339

Adams MP, Hovey RK, Hipsey MR, Bruce LC and others (2016) Feedback between sediment and light for sea-

grass: Where is it important? Limnol Oceanogr 61: 1937–1955
Allen T, Behr J, Bukvic A, Calder RSD and others (2021) Anticipating and adapting to the future impacts of climate change on the health, security and welfare of low elevation coastal zone (LECZ) communities in Southeastern USA. J Mar Sci Eng 9:1196
Aoki LR, McGlathery KJ, Oreska MP (2020) Seagrass restoration reestablishes the coastal nitrogen filter through enhanced burial. Limnol Oceanogr 65:1–12
Aoki LR, McGlathery KJ, Wiberg PL, Oreska MP, Berger AC, Berg P, Orth RJ (2021) Seagrass recovery following marine heat wave influences sediment carbon stocks. Front Mar Sci 7:576784
Berger AC, Berg P, McGlathery KJ, Delgard ML (2020) Long-term trends and resilience of seagrass metabolism: a decadal aquatic eddy covariance study. Limnol Oceanogr 65:1423–1438
Bologna PA, Heck KL Jr (2000) Impacts of seagrass habitat architecture on bivalve settlement. Estuaries 23:449–457
Bologna PA, Heck KL Jr (2002) Impact of habitat edges on density and secondary production of seagrass-associated fauna. Estuaries 25:1033–1044
Boström C, Törnroos A, Bonsdorff E (2010) Invertebrate dispersal and habitat heterogeneity: expression of biological traits in a seagrass landscape. J Exp Mar Biol Ecol 390: 106–117
Bradley K, Houser C (2009) Relative velocity of seagrass blades: implications for wave attenuation in low-energy environments. J Geophys Res Earth Surf 114:F01004
Bricker JD, Monismith SG (2007) Spectral wave-turbulence decomposition. J Atmos Ocean Technol 24:1479–1487
Butman CA (1989) Sediment-trap experiments on the importance of hydrodynamical processes in distributing settling invertebrate larvae in near-bottom waters. J Exp Mar Biol Ecol 134:37–88
Carr J, D'Odorico P, McGlathery K, Wiberg P (2010) Stability and bistability of seagrass ecosystems in shallow coastal lagoons: role of feedbacks with sediment resuspension and light attenuation. J Geophys Res Biogeosci 115: G03011
Carroll JM, Furman BT, Tettelbach ST, Peterson BJ (2012) Balancing the edge effects budget: bay scallop settlement and loss along a seagrass edge. Ecology 93:1637–1647
Chen SN, Sanford LP, Koch E, Shi F, North EW (2007) A nearshore model to investigate the effects of seagrass bed geometry on wave attenuation and suspended sediment transport. Estuar Coasts 30:296–310
Colomer J, Soler M, Serra T, Casamitjana X, Oldham C (2017) Impact of anthropogenically created canopy gaps on wave attenuation in a *Posidonia oceanica* seagrass meadow. Mar Ecol Prog Ser 569:103–116
Dean RG, Dalrymple RA (1991) Water wave mechanics for engineers and scientists. Advanced Series on Ocean Engineering, Vol 2. World Scientific, Singapore
Donatelli C, Ganju NK, Fagherazzi S, Leonardi N (2018) Seagrass impact on sediment exchange between tidal flats and salt marsh, and the sediment budget of shallow bays. Geophys Res Lett 45:4933–4943
Dunic JC, Brown CJ, Connolly RM, Turschwell MP, Côté IM (2021) Long-term declines and recovery of meadow area across the world's seagrass bioregions. Glob Change Biol 27:4096–4109
Eckman JE (1983) Hydrodynamic processes affecting benthic recruitment. Limnol Oceanogr 28:241–257
Eckman JE (1987) The role of hydrodynamics in recruitment, growth, and survival of *Argopecten irradians* (L.) and *Anomia simplex* (D'Orbigny) within eelgrass meadows. J Exp Mar Biol Ecol 106:165–191
El Allaoui N, Serra T, Colomer J, Soler M, Casamitjana X, Oldham C (2016) Interactions between fragmented seagrass canopies and the local hydrodynamics. PLOS ONE 11:e0156264
Fagherazzi S, Wiberg P (2009) Importance of wind conditions, fetch, and water levels on wave-generated shear stresses in shallow intertidal basins. J Geophys Res Earth Surf 114:F03022
Fonseca MS, Koehl MAR (2006) Flow in seagrass canopies: the influence of patch width. Estuar Coast Shelf Sci 67: 1–9
Gacia E, Duarte CM (2001) Sediment retention by a Mediterranean *Posidonia oceanica* meadow: the balance between deposition and resuspension. Estuar Coast Shelf Sci 52: 505–514
Gambi MC, Nowell ARM, Jumars PA (1990) Flume observations on flow dynamics in *Zostera marina* (eelgrass) beds. Mar Ecol Prog Ser 61:159–169
Ghisalberti M, Nepf HM (2002) Mixing layers and coherent structures in vegetated aquatic flows. J Geophys Res Oceans 107:3-1–3-11
Glaspie CN, Seitz RD (2017) Role of habitat and predators in maintaining functional diversity of estuarine bivalves. Mar Ecol Prog Ser 570:113–125
Grant WD, Madsen OS (1979) Combined wave and current interaction with a rough bottom. J Geophys Res Oceans 84:1797–1808
Hansen JCR, Reidenbach MA (2012) Wave and tidally driven flows in eelgrass beds and their effect on sediment suspension. Mar Ecol Prog Ser 448:271–287
Hansen JC, Reidenbach MA (2013) Seasonal growth and senescence of a *Zostera marina* seagrass meadow alters wave-dominated flow and sediment suspension within a coastal bay. Estuar Coasts 36:1099–1114
Hansen JC, Reidenbach MA (2017) Turbulent mixing and fluid transport within Florida Bay seagrass meadows. Adv Water Resour 108:205–215
Infantes E, Orfila A, Simarro G, Terrados J, Luhar M, Nepf H (2012) Effect of a seagrass (*Posidonia oceanica*) meadow on wave propagation. Mar Ecol Prog Ser 456:63–72
Irlandi EA (1997) Seagrass patch size and survivorship of an infaunal bivalve. Oikos 78:511–518
Jing L, Ridd PV (1996) Wave–current bottom shear stresses and sediment resuspension in Cleveland Bay, Australia. Coast Eng 29:169–186
Koch EW, Gust G (1999) Water flow in tide- and wave-dominated beds of the seagrass *Thalassia testudinum.* Mar Ecol Prog Ser 184:63–72
Koch E, Ackerman JD, Verduin J, van Keulen M (2006) Fluid dynamics in seagrass ecology — from molecules to ecosystems. In: Larkum AWD, Orth RJ, Duarte CM (eds) Seagrasses: biology, ecology and conservation. Springer , Dordrecht, p 193–225
Koehl MAR, Hadfield M (2010) Hydrodynamics of larval settlement from a larva's point of view. Integr Comp Biol 50: 539–551
Koehl MAR, Reidenbach MA (2007) Swimming by microscopic organisms in ambient water flow. Exp Fluids 43: 755–768
Lawson SE, Wiberg PL, McGlatherty KJ, Fugate DC (2007) Wind-driven sediment suspension controls light avail-

ability in a shallow coastal lagoon. Estuar Coasts 30: 102–112
Lowe RL, Koseff JR, Monismith SG (2005) Oscillatory flow through submerged canopies: 1. Velocity structure. J Geophys Res Oceans 110:C10016
Lowe RJ, Falter JL, Koseff JR, Monismith SG, Atkinson MJ (2007) Spectral wave flow attenuation within submerged canopies: implications for wave energy dissipation. J Geophys Res Oceans 112:C05018
Luhar M, Coutu S, Infantes E, Fox S, Nepf H (2010) Wave-induced velocities inside a model seagrass bed. J Geophys Res Oceans 115:C12005
McCloskey RM, Unsworth RK (2015) Decreasing seagrass density negatively influences associated fauna. PeerJ 3: e1053
McGlathery KJ, Anderson IC, Tyler AC (2001) Magnitude and variability of benthic and pelagic metabolism in a temperate coastal lagoon. Mar Ecol Prog Ser 216:1–15
McGlathery KJ, Reidenbach MA, D'Odorico P, Fagherazzi S, Pace ML, Porter JH (2013) Nonlinear dynamics and alternative stable states in shallow coastal systems. Oceanography 26:220–231
Nardin W, Larsen L, Fagherazzi S, Wiberg P (2018) Tradeoffs among hydrodynamics, sediment fluxes and vegetation community in the Virginia Coast Reserve, USA. Estuar Coast Shelf Sci 210:98–108
Nepf HM (2012) Flow and transport in regions with aquatic vegetation. Annu Rev Fluid Mech 44:123–142
Nepf HM, Vivoni ER (2000) Flow structure in depth-limited, vegetated flow. J Geophys Res Oceans 105:28547–28557
Nepf HM, Sullivan JA, Zavistoski RA (1997) A model for diffusion with emergent vegetation. Limnol Oceanogr 42: 1735–1745
Oreska MP, McGlathery KJ, Aoki LR, Berger AC, Berg P, Mullins L (2020) The greenhouse gas offset potential from seagrass restoration. Sci Rep 10:7325
Oreska MP, McGlathery KJ, Wiberg PL, Orth RJ, Wilcox DJ (2021) Defining the *Zostera marina* (eelgrass) niche from long-term success of restored and naturally colonized meadows: implications for seagrass restoration. Estuar Coasts 44:396–411
Orth RJ, Heck KL Jr, van Montfrans J (1984) Faunal communities in seagrass beds: a review of the influence of plant structure and prey characteristics on predator–prey relationships. Estuaries 7:339–350
Peterson CH, Summerson H, Duncan P (1984) The influence of seagrass cover on population structure and individual growth rate of a suspension-feeding bivalve, *Mercenaria mercenaria.* J Mar Res 42:123–138
Peterson CH, Luettich RA Jr, Micheli F, Skilleter GA (2004) Attenuation of water flow inside seagrass canopies of differing structure. Mar Ecol Prog Ser 268:81–92
R Core Team (2022) R: a language and environment for statistical computing. R Foundation for Statistical Computing, Vienna
Reidenbach MA, Thomas EL (2018) Influence of the seagrass, *Zostera marina*, on wave attenuation and bed shear stress within a shallow coastal bay. Front Mar Sci 5:397
Reidenbach MA, Timmerman R (2019) Interactive effects of seagrass and the microphytobenthos on sediment suspension within shallow coastal bays. Estuar Coasts 42: 2038–2053
Reidenbach MA, Koseff JR, Koehl MAR (2009) Hydrodynamic forces on larvae affect their settlement on coral reefs in turbulent, wave-driven flow. Limnol Oceanogr 54:318–330
Reidenbach MA, Stocking JB, Szczyrba L, Wendelken C (2021) Hydrodynamic interactions with coral topography and its impact on larval settlement. Coral Reefs 40:505–519
Storlazzi C, Field M, Bothner M (2011) The use (and misuse) of sediment traps in coral reef environments: theory, observations, and suggested protocols. Coral Reefs 30: 23–38
Twomey AJ, O'Brien KR, Callaghan DP, Saunders MI (2020) Synthesising wave attenuation for seagrass: drag coefficient as a unifying indicator. Mar Pollut Bull 160:111661
Verduin JJ, Backhaus JO (2000) Dynamics of plant–flow interactions for the seagrass *Amphibolis antarctica*: field observations and model simulations. Estuar Coast Shelf Sci 50:185–204
Wiberg PL, Sherwood CR (2008) Calculating wave-generated bottom orbital velocities from surface-wave parameters. Comput Geosci 34:1243–1262
Widdows J, Pope ND, Brinsley MD, Asmus H, Asmus RM (2008) Effects of seagrass beds (*Zostera noltii* and *Z. marina*) on near-bed hydrodynamics and sediment resuspension. Mar Ecol Prog Ser 358:125–136
Wilson FS (1990) Temporal and spatial patterns of settlement: a field study of molluscs in Bogue Sound, North Carolina. J Exp Mar Biol Ecol 139:201–220
Yarnall AH, Byers JE, Yeager LA, Fodrie FJ (2022) Comparing edge and fragmentation effects within seagrass communities: a meta-analysis. Ecology 103:e3603
Zhang Y, Nepf H (2019) Wave-driven sediment resuspension within a model eelgrass meadow. J Geophys Res Earth Surf 124:1035–1053
Zhu Q, Wiberg PL, Reidenbach MA (2021) Quantifying seasonal seagrass effects on flow and sediment dynamics in a Back-Barrier Bay. J Geophys Res Oceans 126: e2020JC016547
Zhu Q, Wiberg PL, McGlathery KJ (2022) Seasonal growth and senescence of seagrass alters sediment accumulation rates and carbon burial in a coastal lagoon. Limnol Oceanogr 67:1931–1942

Editorial responsibility: Mirta Teichberg, Woods Hole, Massachusetts, USA
Reviewed by: 3 anonymous referees

Submitted: June 11, 2023
Accepted: January 30, 2024
Proofs received from author(s): March 18, 2024